Chapter 5
Visco-plastic and Damage Characterization of Sheet Metals for Railway Crash Applications

Valentina Arrà, Mattia Utzeri, Gianluca Chiappini, Marco Sasso, and Alberto Perticone

Abstract This work investigates the visco-plastic behavior and damage evolution of stainless-steel sheet metals for railway crash applications under varying strain rates. The study combines quasi-static and dynamic tests, using a universal testing machine and a Split Hopkinson Bar (SHB), to evaluate the material response across a range of strain rates. The objective is to investigate how the yield surface evolves as a function of strain rate, evaluating the material's sensitivity to varying loading conditions. Additionally, the study aims to understand how these variations influence the failure strain and ductility, providing essential insights for enhancing the reliability of crashworthiness simulations.

To obtain a detailed description of the fracture locus, mechanical tests will be conducted on specimens with varying geometries, designed to induce both uniaxial and multiaxial loading conditions. This approach captures a wide range of stress states, enabling the calibration of the fracture locus as a function of triaxiality and Lode parameter to better understand how damage evolves under different strain rates.

Numerical simulations of the experiments were setup for calibration and validation purposes to ensure that the numerical models accurately represent the material behavior.

The plasticity model is identified using an inverse Finite Element (FE) approach, based on experimental data from both quasi-static and dynamic tests. The visco-plastic response of the sheet metals is then described using the Johnson-Cook and Cowper-Symonds models.

To replicate the damage initiation and progression, appropriate damage models are selected and implemented in ABAQUS FE software. The calibration process is based on a comparison between the simulated and experimental results, iteratively adjusting the model parameters until an optimal match is obtained. This iterative fitting allows for a comprehensive representation of the material behavior, capturing the influence of strain rate and stress state on the yield surface and fracture locus.

Keywords High strain rate · Hopkinson Bar · Stress Triaxiality · Ductile damage

Introduction

This study focuses on the mechanical characterization of 550W steel through static and dynamic tests, integrated with FEM simulations using Abaqus/CAE. The main objective is to calibrate a ductile damage model to predict material failure based on triaxiality and strain rate.

The importance of this research lies in the potential to improve the performance of structural materials used in high-stress applications, such as energy absorption systems for railway carriages [1, 2], by optimizing component safety and durability.

Valentina Arrà · Mattia Utzeri · Marco Sasso
Department of Industrial Engineering and Mathematical SciencesUniversità Politecnica delle Marche, 60131, Ancona - Italy
e-mail: v.arra@pm.univpm.it; m.utzeri@staff.univpm.it; m.sasso@univpm.it

Gianluca Chiappini
Università Telematica eCampusNovedrate, Como, 22060 – Italy
e-mail: g.chiappini@staff.univpm.it

Alberto Perticone
Hitachi Rail STS SpaCiliegiole, 51100 Pistoia – Italy
e-mail: alberto.perticone.ayes@hitachirail.com

Emily Retzlaff et al. (eds.), *Mechanics of Additive & Advanced Manufacturing, Inverse Methods and Machine Learning, Vol. 5*,
Conference Proceedings of the Society for Experimental Mechanics Series, https://doi.org/10.13052/97887-438-0831-2_5

Understanding the mechanical behavior of 550W steel fits into a broader context of studies analyzing the relationship between triaxiality and ductile fracture. Models like Rice-Tracey [3], Hancock-Mackenzie [3] and Bao-Wierzbicki [5] have highlighted the correlation of ductility with stress triaxiality. Bai-Wierzbicki [6] and Dunand-Mohr [7] studied the effect of Lode angle. Since the seminal work of Johnson-Cook [8], another important parameter is known to be represented by strain rate, where triaxiality and strain rates are considered in an uncoupled way; several damage models account for such parameters thus describing a fracture locus or fracture surface as a function of Lode angle, triaxiality and strain rate [9]. Further works included the temperature effect, both in terms of initial temperature and self-heating due to plastic work [10].

This research adopts a mixed experimental-numerical approach, calibrating the Bao-Wierzbicki [5] model based on collected experimental data and validated through FEM simulations. Differently from Johnson-Cook model [8], the effect of strain rate will be considered with a non-monotonous polynomial law.

Methodology

The experimental tests were conducted on specimens of various geometries to achieve different stress states. The methodology involves five phases: i) specimen preparation, ii) test execution, iii) data acquisition and post-processing, iv) visco-plastic modeling, v) damage modeling. Four specimen geometries, shown in Figure 1, were extracted by laser cutting from 4 mm thick plates of 550 weathering steel, to be tested with strain rates ranging from 10^{-2} to 10^{3} s^{-1}, [5].

The experimental tests were executed by an electro-mechanical testing machine (Zwick-Roell® Z050) and by a direct tension split Hopkinson Bar [12], capable of reaching strain rates up to 1000 s^{-1}. During the tests, key parameters like deformation, load, and failure mode were monitored using strain gauges and Digital Image Correlation (DIC) techniques. In

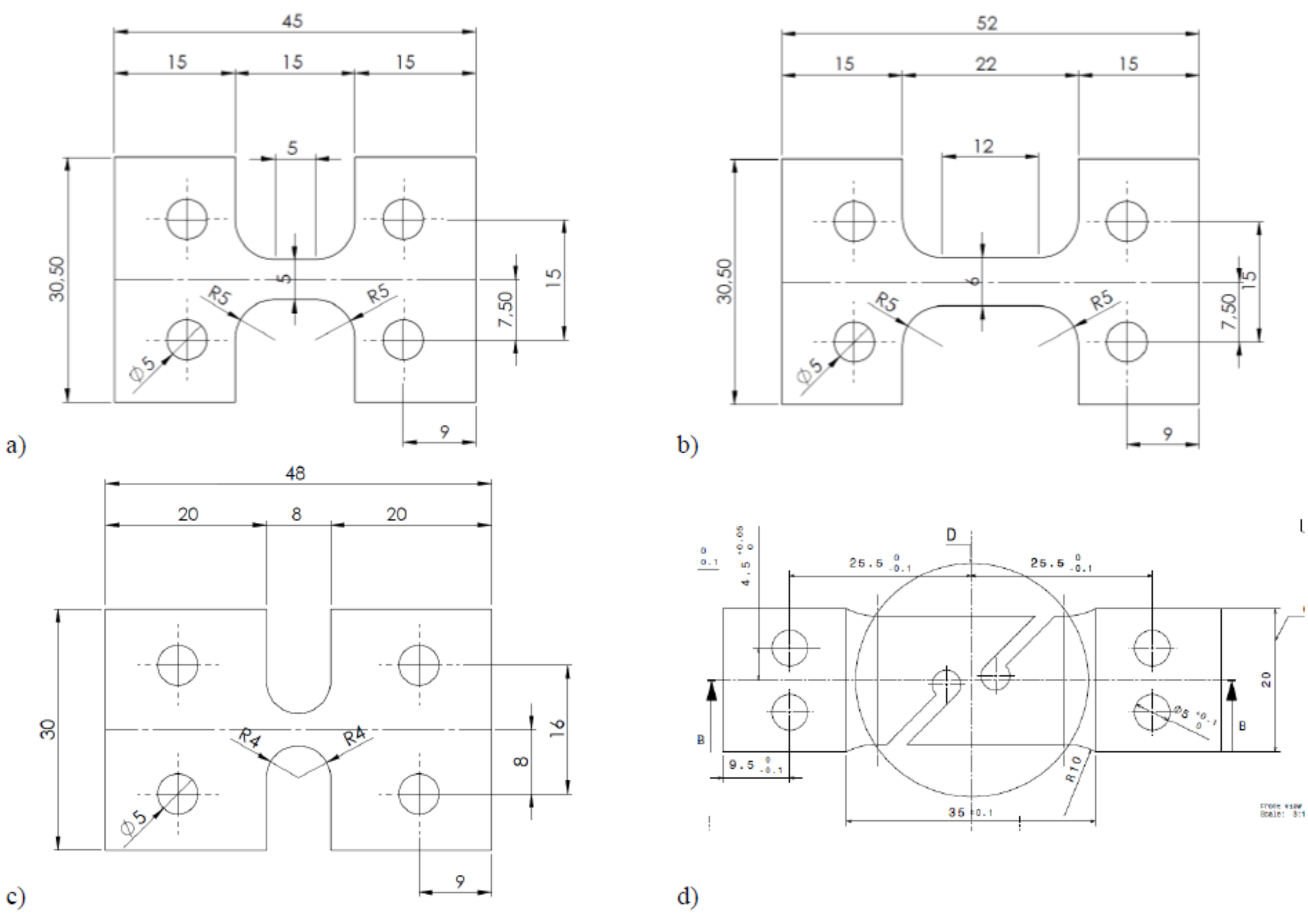

Fig. 1 Geometries of tested sample; a,b) P1 and P2 geometries for uniaxial tests at intermediate triaxiality; c) P3 notched geometry for high triaxiality; d) D10 Driemeier geometry [11] for low triaxiality testsbroken

particular, engineering uniaxial stress-strain curves were obtained for different strain rates using the P1 and P2 geometries; then, the average strain computed in the necking section from DIC analyses was used to convert the engineering data into first-attempt true stress-strain curves. A mixed analytical-numerical procedure was implemented: FEM simulations were repeated varying material parameters according to an optimization scheme, where deviations between numerical and experimental load-displacement curves are minimized. Figure 2 shows the 3D meshed models developed in Abaqus/Explicit ® software; the mesh size of all models was 0.25mm in the gauge area.

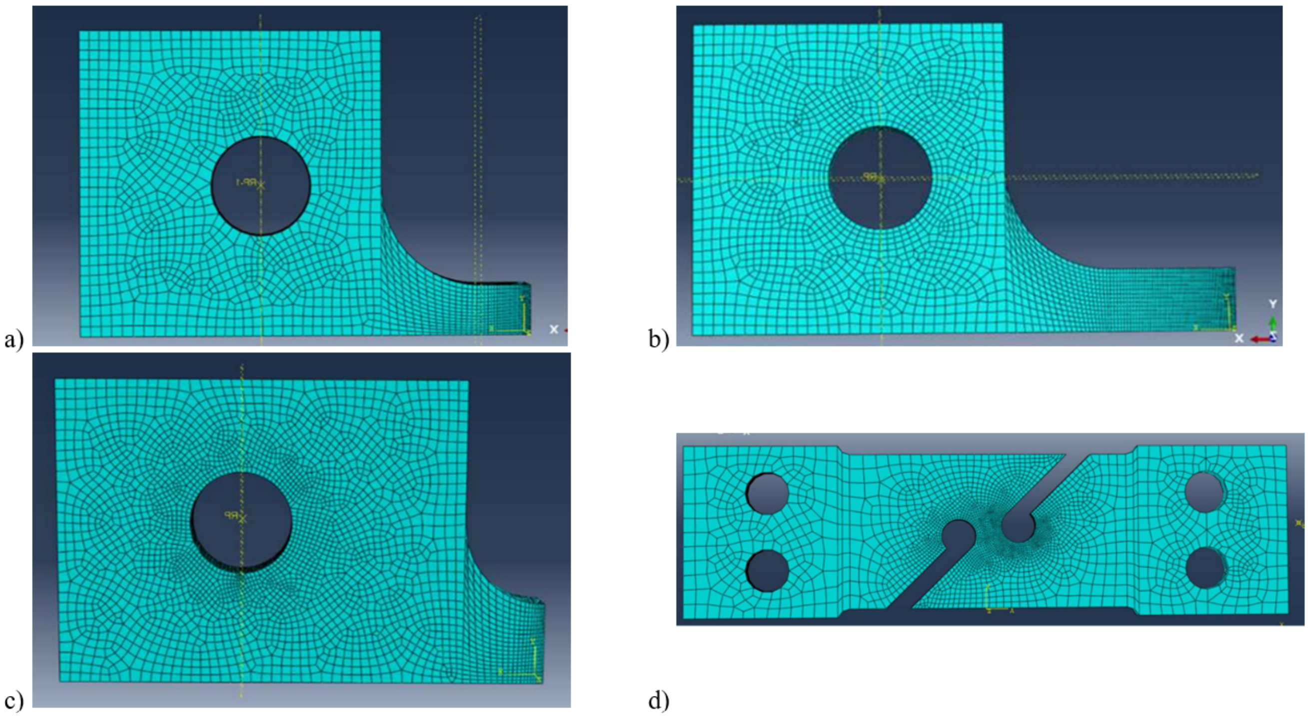

Fig. 2 FE models in Abaqus/Explicit; a) P1 geometry, b) P2 geometry, c) P3 notched geometry, d) D10 geometry

The adopted visco-plastic law is given by the Voce's hardening law, combined with the Johnson-Cook strain rate dependency term [13], which was input in tabular form as material mechanical properties. The equation is:

$$\sigma = \{\sigma_0 + R_0 \cdot \varepsilon_{pl} + R_\infty \left[1 - exp\left(-b \cdot \varepsilon_{pl}\right)\right]\} \cdot \left[1 + q \cdot ln\left(\dot{\varepsilon}/\dot{\varepsilon_0}\right)\right] \tag{1}$$

After the visco-plastic model was calibrated, the same simulations were used to extract the characteristic parameters such as stress triaxiality and effective strain rate at the core of the samples; these data were used for the definition of a fracture locus in the (T, $\dot{\varepsilon}$, ε_f) space; in particular, the Bao-Wierzbicki model was first calibrated based on quasi-static results. The equation is divided into three regions, the first corresponding to shear cracking, the third to void growth, and the second corresponding to a mixed failure mode:

$$\begin{cases} region\ I: \ \varepsilon_f = a(T + 1/3)^b \\ region\ II: \ \varepsilon_f = cT^2 + dT + e \\ region\ III: \ \varepsilon_f = fT^{-1} \end{cases} \tag{2}$$

Then, the strain rate dependency was considered by a polynomial law of second and third-order, thus to define a 3D fracture surface:

$$f(T, \log(\dot{\varepsilon})) = c_1 + c_2 T + c_3 \log(\dot{\varepsilon}) + c_4 T^2 + c_5 T \log(\dot{\varepsilon}) + c_6 \log(\dot{\varepsilon})^2 \tag{3a}$$

$$f(T, \log(\dot{\varepsilon})) = c_1 + c_2 T + c_3 \log(\dot{\varepsilon}) + c_4 T^2 + c_5 T \log(\dot{\varepsilon}) + c_6 \log(\dot{\varepsilon})^2 + c_7 T^3 + c_8 T^2 \log(\dot{\varepsilon}) + c_9 T \log(\dot{\varepsilon})^2 + c_{10} \log(\dot{\varepsilon})^3 \tag{3b}$$

The coefficients were found by minimizing the distance between the points and the surface.

Results

The engineering curves of uniaxial tests at different strain rates on P1 and P2 samples are shown in Figure 3. The ductility of the material, in terms of strain to failure, is observed to be constant between quasi-static and intermediate strain rate; at higher strain rates, the ductility was found to decrease at approximately 500 s^{-1}, whereas it increases nearly to the quasi-static values at 1000 s^{-1}.

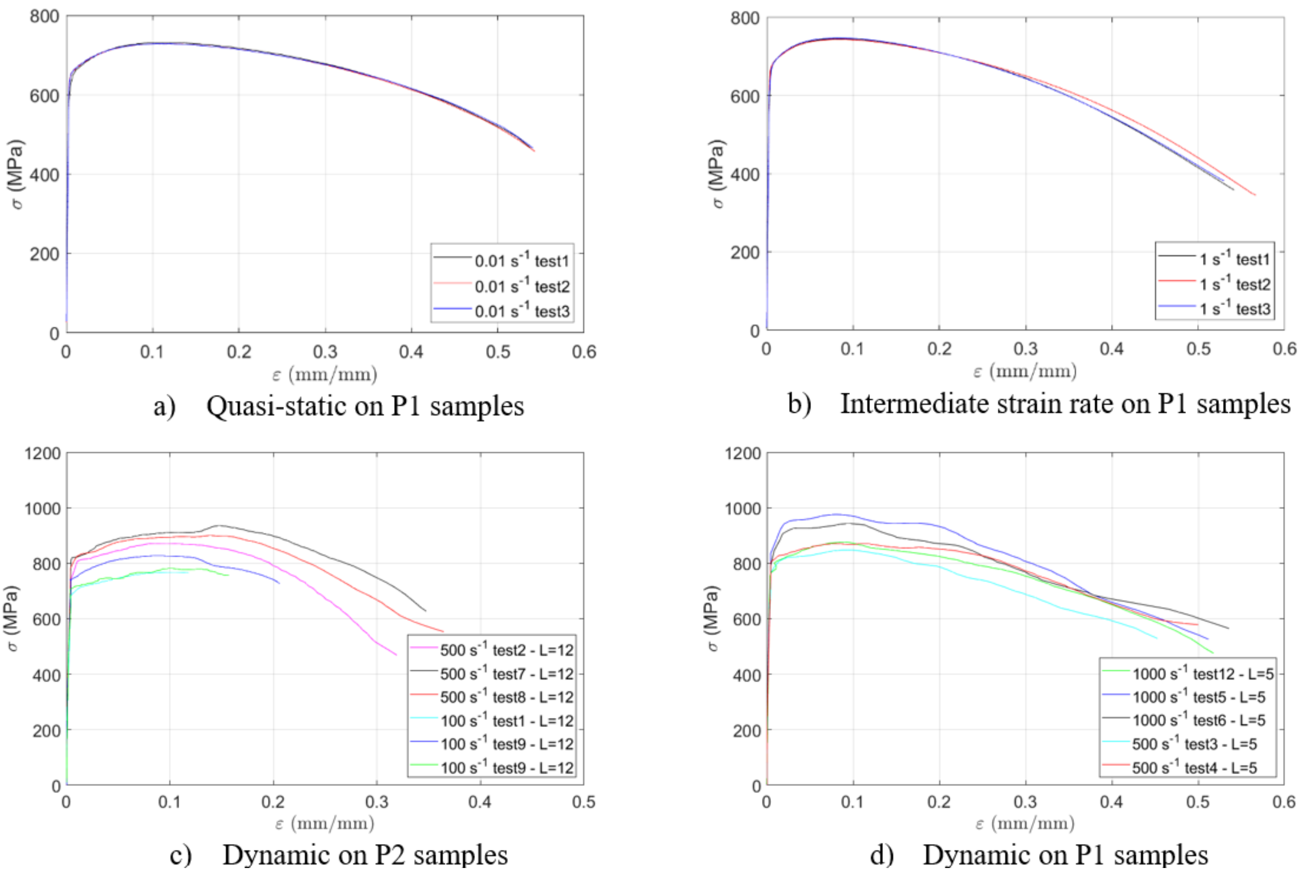

Fig. 3 FE models in Abaqus/Explicit; a) P1 geometry, b) P2 geometry, c) P3 notched geometry, d) D10 geometry

The results of uniaxial tests at different strain rates revealed that the strain rate dependence is indeed well described by a polyline with double slope in the double-logarithmic plane, as shown in Figure 4. It is noted that the strain rate affected material behavior mainly above a threshold strain rate $[\dot{\varepsilon}_0]$ of 155 s^{-1}. The parameters of the Voce's hardening law are reported in Table 1. The global material behavior was input as a tabular material card into Abaqus material properties.

Table 1 Voce's hardening parameters

σ_0 [MPa]	R_0 [MPa]	R_∞ [MPa]	b
644	260	226	7.63

Considering the visco-plastic behavior of the material, the numerical simulations showed a very good agreement with experimental data, in terms of reconstructed load-displacement curves, with deviations as low as 2.5%. Figures 5 show the curves of the P1 geometries tested at different strain rates. A similar agreement, not reported here for the sake of brevity, was found for the P3 Notched and D10 geometries.

After having validated the behavior of visco-plastic constitutive model, attention was paid to the deformation at failure. The average stress triaxiality and the equivalent plastic strain at the instant of failure was computed in the most critical elements of each model. The P1 and P2 samples showed the highest plastic strain at failure at the core elements. Notched specimens exhibited localized deformation concentrations in the notched area, with a reduced strain to failure, confirming the

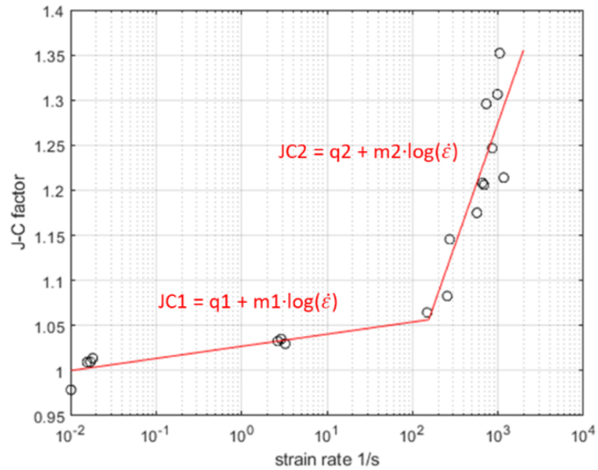

Fig. 4 strain rate dependency of material strength

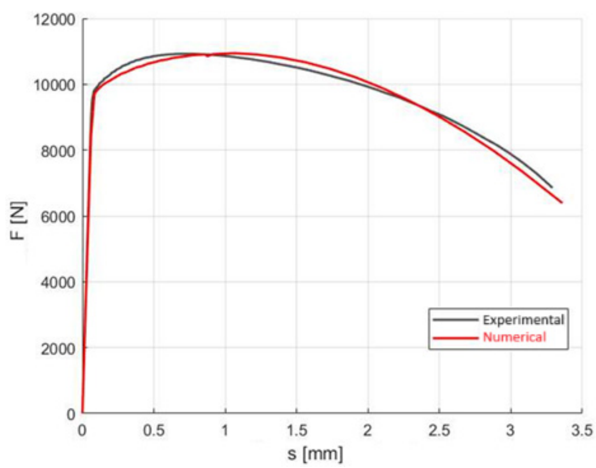

a)

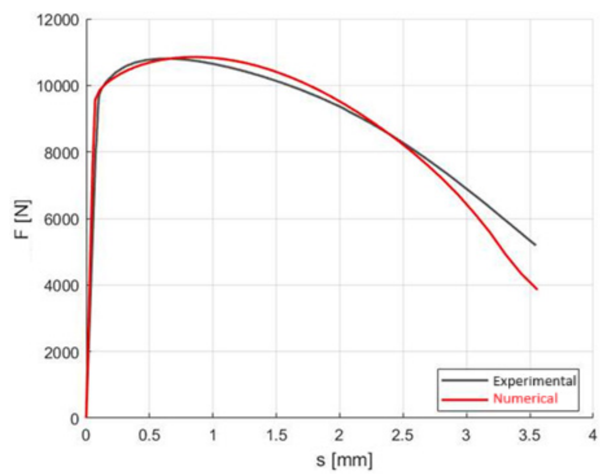

b)

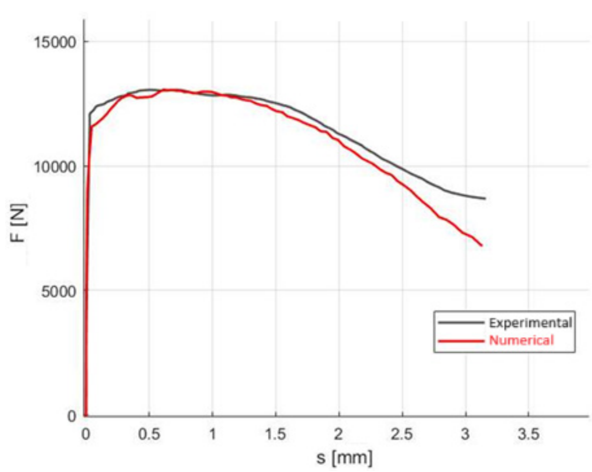

c)

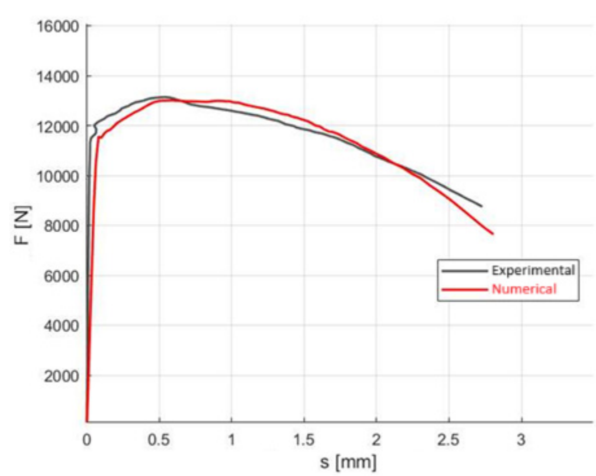

d)

Fig. 5 Comparison of experimental and numerically reconstructed load-displacement curves for tests on P1 samples at different strain rates; a) 10^{-2} s^{-1}; b) 10^{0} s^{-1}; c) $5{\cdot}10^{2}$ s^{-1}; d) $10^{3}s^{-1}$

correlation between triaxiality and fracture behavior. Dremeier specimen revealed a strain to failure slightly lower than P1 and P2. Consequently, the comparison between the results obtained with empirical ductile damage models showed that the Bao-Wierzbicki model better represents the material's behavior compared to the Rice-Tracey or Cockcroft-Latham models. Figure 6a shows the trend of strain to failure as a function of stress triaxiality T in quasi-static conditions. The extension to strain rate as a third axis leads to the bi-cubic surface given in Figure 6b.

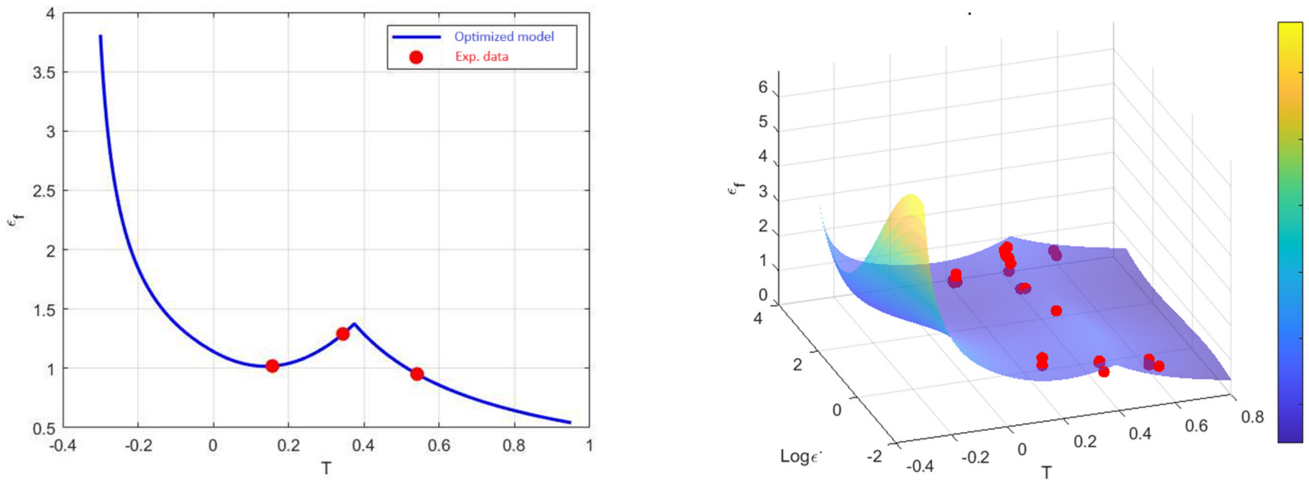

a) b)

Fig. 6 Calibrated Bao-Wierzbicki: a) application to quasi-static data; b) extension to strain rate effect by polynomial surface

The results demonstrate the validity of the chosen approach to describe the behavior of 550W steel under dynamic loads. The FEM methodology enabled the investigation of phenomena that are not directly measurable in the laboratory, such as the evolution of strain and stress tensors and the fracture surface. The Bao-Wierzbicki damage model showed high predictive capability for fracture in complex loading states. Nevertheless, Figures 7 show that the trend of the material ductility with strain rate is not very smooth; as a result, the simple quadratic law appears to be not well representative, whereas the cubic law is affected by a certain overfitting effect; further investigation is needed, especially at an intermediate strain rate.

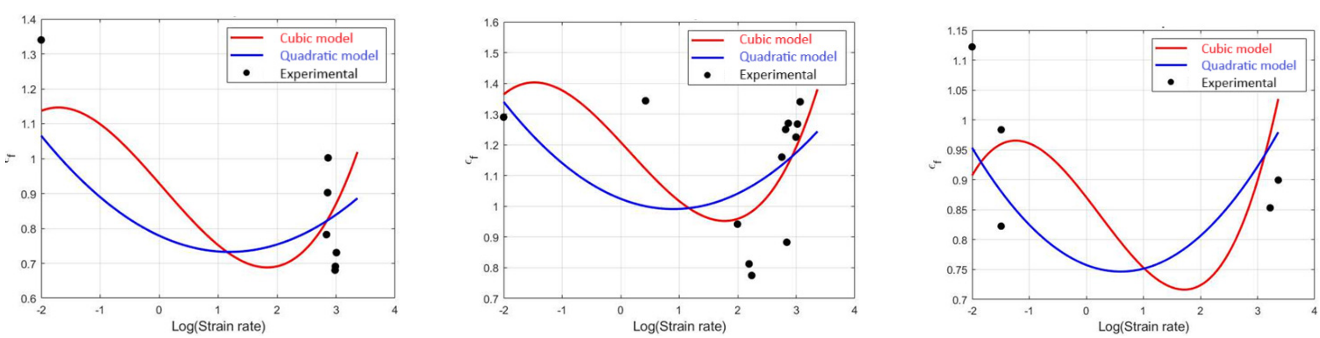

a) b) c)

Fig. 7 Trend of strain to failure at different strain rates and triaxiality values according to quadratic or cubic surface fitting: a) T = 0.14 (Driemeier samples), b) T = 0.34 (P1 and P2 samples), c) T = 0.54 (P3 notched samples)

Conclusion

The research confirms the reliability of the adopted approach in predicting the behavior of 550W steel under operational conditions and provides a significant contribution to the modeling of ductile damage in structural materials. The methodology adopted allowed for an accurate description of the material's behavior and successful calibration of the Bao-Wierzbicki damage model. The results can be applied to the railway industry to improve the performance of crash absorbers.

Future perspectives include the extension of tests to intermediate strain rates, and the implementation of an advanced damage model to account for varying strain rates with a more complex behavior rather than the simple quadratic or cubic law here adopted.

Acknowledgments The authors would like to express their gratitude to Hitachi Rail STA S.p.A., Ciliegiole, 51100 Pistoia – Italy for commissioning and supporting this research work. In particular, we thank them for providing the material, and for their valuable collaboration and scientific contributions during the various phases of the project.

References

1. Seung, R.K., and Jeong S.K., (2008) A study on strain rate effect in collision analysis of rolling stock, International Journal of Modern Physics B, 22:09n11, 1423-1430
2. Xie S., Du X., Zhou H., Wang D., Feng Z., (2020) Analysis of the crashworthiness design and collision dynamics of a subway train. Proceedings of the Institution of Mechanical Engineers, Part F: Journal of Rail and Rapid Transit 234(10):1117
3. Rice, J.R. and Tracey, D.M. (1969). On the ductile enlargement of voids in triaxial stress fields. Journal of the Mechanics and Physics of Solids.
4. Hancock J.W., and Mackenzie A.C., (1976). On the mechanisms of ductile failure in high-strength steels subjected to multi-axial stress-states. Journal of the Mechanics and Physics of Solids 24: 147–160
5. Bao, Y., and Wierzbicki, T. (2004). A Comparative Study on Fracture Models for Ductile Metals. International Journal of Mechanical Sciences.
6. Bai, Y., and Wierzbicki T (2008). A new model of metal plasticity and fracture with pressure and Lode dependence. International Journal of Plasticity 24: 1071–1096.
7. Dunand, M., and Mohr, D., (2011). On the predictive capabilities of the shear modified Gurson and the modified Mohr-Coulomb fracture models over a wide range of stress triaxialities and Lode angle. Journal of the Mechanics and Physics of Solids 59: 1374–1394.
8. Johnson, G.R. and Cook, W.H. (1985). Fracture characteristics of three metals subjected to various strains, strain rates, temperatures and pressures. Engineering Fracture Mechanics, 21:31–48.
9. Cortese L., Coppola T., Campanelli F., Campana F., and Sasso M., (2013). Prediction of ductile failure in materials for onshore and offshore pipeline applications, International Journal of Damage Mechanics, 23(1): 104-123
10. Cortis, G., Nalli, F., Sasso, M., Cortese, L., and Mancini, E., (2022). Effects of Temperature and Strain Rate on the Ductility of an API X65 Grade Steel, Applied Sciences Volume 12(5):2444
11. Brünig M, Chyra O, Albrecht D, Driemeier L., and Alves M. (2008). A ductile damage criterion at various stress triaxialities International Journal of Plasticity (24) 1731-55
12. Mancini, E.; Sasso, M.; Rossi, M.; Chiappini, G.; Newaz, G.; Amodio D., (2015). Design of an Innovative System for Wave Generation in Direct Tension–Compression Split Hopkinson Bar. J. Dyn. Behav. Mater. (1) 201–213
13. Johnson, G.R., and Cook, W.H. (1983). A constitutive model and data for metals subjected to large strains, high strain rates and high temperatures, Proceedings of the 7th International Symposium of Ballistics.